Biomedical Optics EXPRESS

Assessment of local structural disorders of the bladder wall in partial bladder outlet obstruction using polarized light imaging

Sanaz Alali,[1,*] Karen J. Aitken,[2] Annette Schröder,[2] Adam Gribble,[1] Darius J. Bagli,[2] and I. Alex Vitkin[1,3]

[1]*University of Toronto, Division of Biophysics and Bioimaging, Ontario Cancer Institute/University Health Network and Department of Medical Biophysics, 610 University Avenue, Toronto, Ontario M5G 2M9 Canada*
[2]*University of Toronto, Division of Urology, Developmental & Stem Cell Biology, Sick Kids Hospital, 555 University Avenue, Toronto, Ontario M5G 1X8 Canada*
[3]*University of Toronto, Department of Radiation Oncology, 610 University Avenue, Toronto, Ontario M5G 2M9 Canada*
[*]*Sanaz.alali@mail.utoronto.ca*

Abstract: Partial bladder outlet obstruction causes prominent morphological changes in the bladder wall, which leads to bladder dysfunction. In this paper, we demonstrate that polarized light imaging can be used to identify the location of obstruction induced structural changes that other imaging modalities fail to detect. We induced 2-week and 6-week partial outlet obstruction in rats, harvested obstructed bladders, then measured their retardances while distended to high pressures and compared them to controls. Our results show that the retardance of the central part of the ventral side (above the ureters) closer to the urethra can be used as a potential metric of the distending bladder obstruction.

OCIS codes: (170.7230) Urology; (170.0110) Imaging systems; (170.4580) Optical diagnostics for medicine.

References and links

1. D. E. Irwin, Z. S. Kopp, B. Agatep, I. Milsom, and P. Abrams, "Worldwide prevalence estimates of lower urinary tract symptoms, overactive bladder, urinary incontinence and bladder outlet obstruction," BJU Int. **108**(7), 1132–1138 (2011).
2. J. Wein, *Campbell-Walsh Urology*, 9th ed., (Elsevier, 2007).
3. K. J. Aitken and D. J. Bägli, "The bladder extracellular matrix. Part I: architecture, development and disease," Nat. Rev. Urol. **6**(11), 596–611 (2009).
4. A. Schröder, T. P. Kirwan, J. X. Jiang, K. J. Aitken, and D. J. Bägli, "Rapamycin attenuates bladder hypertrophy during long-term outlet obstruction in vivo: tissue, matrix and mechanistic insights," J. Urol. **189**(6), 2377–2384 (2013).
5. A. Tubaro, C. De Nunzio, A. Trucchi, G. Palleschi, and L. Miano, "The effect of bladder outlet obstruction treatment on ultrasound-determined bladder wall thickness," Rev. Urol. **7**(Suppl 6), S35–S42 (2005).
6. P. Dewan and M. E. Mitchell, *Bladder Augmentation* (Arnold, 2000).
7. C. Andrew, A. Novick, J. S. Jones, and I. S. Gill, *Operative Urology at the Cleveland Clinic* (Humanpress, 2006).
8. J. J. Yoo, J. Meng, F. Oberpenning, and A. Atala, "Bladder augmentation using allogenic bladder submucosa seeded with cells," Urology **51**(2), 221–225 (1998).
9. G. S. Jack, R. Zhang, M. Lee, Y. Xu, B. M. Wu, and L. V. Rodríguez, "Urinary bladder smooth muscle engineered from adipose stem cells and a three dimensional synthetic composite," Biomaterials **30**(19), 3259–3270 (2009).
10. R. L. Heise, J. Ivanova, A. Parekh, and M. S. Sacks, "Generating elastin-rich small intestinal submucosa-based smooth muscle constructs utilizing exogenous growth factors and cyclic mechanical stimulation," Tissue Eng. Part A **15**(12), 3951–3960 (2009).
11. S. Korossis, F. Bolland, J. Southgate, E. Ingham, and J. Fisher, "Regional biomechanical and histological characterisation of the passive porcine urinary bladder: Implications for augmentation and tissue engineering strategies," Biomaterials **30**(2), 266–275 (2009).
12. J. Nagatomi, K. K. Toosi, J. S. Grashow, M. B. Chancellor, and M. S. Sacks, "Quantification of bladder smooth muscle orientation in normal and spinal cord injured rats," Ann. Biomed. Eng. **33**(8), 1078–1089 (2005).
13. S. Alali, K. J. Aitken, A. Schröder, D. J. Bagli, and I. A. Vitkin, "Optical assessment of tissue anisotropy in *ex vivo* distended rat bladders," J. Biomed. Opt. **17**(8), 086010 (2012).

#200672 - $15.00 USD Received 6 Nov 2013; revised 9 Jan 2014; accepted 13 Jan 2014; published 27 Jan 2014

14. M. Belal and P. Abrams, "Noninvasive methods of diagnosing bladder outlet obstruction in men. Part 1: Nonurodynamic approach," J. Urol. **176**(1), 22–28 (2006).
15. S. L. Jacques, J. C. Ramella-Roman, and K. Lee, "Imaging skin pathology with polarized light," J. Biomed. Opt. **7**(3), 329–340 (2002).
16. M. F. G. Wood, N. Ghosh, M. A. Wallenburg, S. H. Li, R. D. Weisel, B. C. Wilson, R. K. Li, and I. A. Vitkin, "Polarization birefringence measurements for characterizing the myocardium, including healthy, infarcted, and stem-cell-regenerated tissues," J. Biomed. Opt. **15**(4), 047009 (2010).
17. M. A. Wallenburg, M. F. G. Wood, N. Ghosh, and I. A. Vitkin, "Polarimetry-based method to extract geometry-independent metrics of tissue anisotropy," Opt. Lett. **35**(15), 2570–2572 (2010).
18. G. Jarry, F. Henry, and R. Kaiser, "Anisotropy and multiple scattering in thick mammalian tissues," J. Opt. Soc. Am. A **17**(1), 149–153 (2000).
19. A. Pierangelo, A. Nazac, A. Benali, P. Validire, H. Cohen, T. Novikova, B. H. Ibrahim, S. Manhas, C. Fallet, M. R. Antonelli, and A. D. Martino, "Polarimetric imaging of uterine cervix: a case study," Opt. Express **21**(12), 14120–14130 (2013).
20. X. Li and G. Yao, "Mueller matrix decomposition of diffuse reflectance imaging in skeletal muscle," Appl. Opt. **48**(14), 2625–2631 (2009).
21. S. Lu and R. A. Chipman, "Interpretation of Mueller matrices based on polar decomposition," J. Opt. Soc. Am. A **13**(5), 1106–1113 (1996).
22. M. F. G. Wood, N. Ghosh, E. H. Moriyama, B. C. Wilson, and I. A. Vitkin, "Proof-of-principle demonstration of a Mueller matrix decomposition method for polarized light tissue characterization in vivo," J. Biomed. Opt. **14**(1), 014029 (2009).
23. M. S. Damaser, K. Brzezinski, and P. A. Longhurst, "Filling Mechanics of obstructed and de-obstructed Rat Urinary Bladders," Neurourol. Urodyn. **18**(6), 659–671 (1999).
24. M. S. Elkelini, K. Aitken, D. J. Bagli, and M. M. Hassouna, "Effects of doxycycline on voiding behaviour of rats with bladder outlet obstruction," BJU Int. **103**(4), 537–540 (2009).
25. K. J. Aitken, G. Block, A. Lorenzo, D. Herz, N. Sabha, O. Dessouki, F. Fung, M. Szybowska, L. Craig, and D. J. Bägli, "Mechanotransduction of extracellular signal-regulated kinases 1 and 2 mitogen-activated protein kinase activity in smooth muscle is dependent on the extracellular matrix and regulated by matrix metalloproteinases," Am. J. Pathol. **169**(2), 459–470 (2006).
26. K. J. Aitken, C. Tolg, T. Panchal, B. Leslie, J. Yu, M. Elkelini, N. Sabha, D. J. Tse, A. J. Lorenzo, M. Hassouna, and D. J. Bägli, "Mammalian target of rapamycin (mTOR) induces proliferation and de-differentiation responses to three coordinate pathophysiologic stimuli (mechanical strain, hypoxia, and extracellular matrix remodeling) in rat bladder smooth muscle," Am. J. Pathol. **176**(1), 304–319 (2010).
27. B. O. Backhaus, M. Kaefer, K. M. Haberstroh, K. Hile, J. Nagatomi, R. C. Rink, M. P. Cain, A. Casale, and R. Bizios, "Alterations in the molecular determinants of bladder compliance at hydrostatic pressures less than 40 cm. H2O," J. Urol. **168**(6), 2600–2604 (2002).
28. J. Zeng, K. Xie, C. Jiang, J. Mo, and S. Lindström, "Bladder mechanoreceptor changes after artificial bladder outlet obstruction in the anesthetized rat," Neurourol. Urodyn. **31**(1), 178–184 (2012).
29. A. Arner, R. Sjuve Scott, H. Haase, I. Morano, and B. Uvelius, "Intracellular calcium in hypertrophic smooth muscle from rat urinary bladder," Scand. J. Urol. Nephrol. **41**(4), 270–277 (2007).
30. D. Burmeister, T. AbouShwareb, R. D'Agostino, Jr., K. E. Andersson, and G. J. Christ, "Impact of partial urethral obstruction on bladder function: Time dependent changes and functional correlates of altered expression of Ca2+ signaling regulators," Press. Am. J. Physiol. Renal. **302**(12), F1517–F1528 (2012).
31. J. Chen, B. A. Drzewiecki, W. David Merryman, and J. C. Pope, "Murine bladder wall biomechanics following partial bladder obstruction," J. Biomechanics **46,** 2752–2755 (2013).
32. M. B. Siroky, "The aging bladder," Rev. Urol. **6**(Suppl 1), S3–S7 (2004).
33. S. Matsumoto, P. Chichester, B. A. Kogan, and R. M. Levin, "Structural and vascular response of normal and obstructed rabbit whole bladders to distension," Urology **62**(6), 1129–1133 (2003).
34. S. A. Capello, E. Chieh-Lung Chou, and P. A. Longhurst, "Regional differences in responses of rabbit detrusor to electrical and adrenergic stimulation: influence of outlet obstruction," BJU Int. **95**(1), 157–162 (2005).
35. K. Sugimoto, S. Matsumoto, H. Ito, and H. Uemura, "Effect of partial bladder outlet obstruction on the morphology of elastin in rabbit bladder smooth muscle," Lower Urinary Tract Symptoms **2**, 71–75 (2010).
36. J. Qi, C. Barrière, T. C. Wood, and D. S. Elson, "Polarized multispectral imaging in a rigid endoscope based on elastic light scattering spectroscopy," Biomed. Opt. Express **3**(9), 2087–2099 (2012).
37. A. Myakov, L. Nieman, L. Wicky, U. Utzinger, R. Richards-Kortum, and K. Sokolov, "Fiber optic probe for polarized reflectance spectroscopy in vivo: Design and performance," J. Biomed. Opt. **7**(3), 388–397 (2002).

1. Introduction

Partial bladder outlet obstruction (PBO) will affect about 1.1 billion people in 2018 [1]. PBO is the blockage of the outlet, which may arise from overgrowth of the prostate, posterior urethral valves or neurogenic bladder [2]. The outlet blockage will result in excessive urine accumulation in the bladder and high volume or high pressure that leads to the detrusor muscle hypertrophy and hyperplasia over time [2,3]. Other bladder wall properties affected by prolonged or chronic obstruction, indicated by microscopy studies, include decreased angiogenesis and changes in the extracellular matrix, including fibrosis (increase in elastin

#200672 - $15.00 USD Received 6 Nov 2013; revised 9 Jan 2014; accepted 13 Jan 2014; published 27 Jan 2014

and collagen deposition) and elastin break-down into small fibers [3,4]. These compositional and morphological changes in the bladder wall tissue impair the bladder's capability to contract and distend efficiently [2–5]. Due to this resultant bladder dysfunction, PBO patients often suffer from urinary tract infection, incontinence and kidney failure [1–3,5]. In many cases, the bladder wall damage is irreversible, necessitating augmentation surgery [6]. Augmentation cystoplasty is the procedure of replacing the bladder wall, frequently the dome region, with parts of the autologous gastrointestin/bowel wall or artificially engineered tissue [6–10]. However, it is known that regional structural organization and biomechanical properties of the bladder wall are region specific, and vary spatially depending on the anatomical location of the tissue [11–13]. Hence, augmentation procedures should be optimized to be specifically targeted to regions with the most morphological alterations. Current *in vivo* imaging methods such as x-ray, ultrasound and MRI can only identify anatomical changes in the bladder that are spatially nearly uniform throughout the bladder wall [5,14]. Therefore, new *in vivo* imaging techniques are needed that can identify the regions with the most pronounced morphological changes, to localize and optimize augmentation procedures.

One of the morphological characteristics of tissue is its anisotropy (directionality), which arises from the micro-structural organization (alignment) of muscle fibers and extracellular matrix components. One appealing method to quantitatively assess anisotropy of biological tissues is polarized light imaging [15–20]. Polarized light imaging can measure the media's anisotropy in terms of optical retardance, which is proportional to the tissue thickness (sampling volume) and birefringence. However, extracting information from polarized light after interaction with biological tissues is challenging, because tissues are turbid and light depolarizes quickly after multiple scattering events during propagation [15–22]. However, birefringence of optically thick tissues can be obtained by using Mueller matrix decomposition, which separates different optical polarization effects [15–22]. For instance, using polarized light imaging and Mueller matrix decomposition we previously demonstrated regional anisotropy differences in normal *ex vivo* rat bladders under different distension pressures [13]. Rats have been widely used as PBO models since they exhibit similar tissue complications and urodynamics to humans [23–30]. In this study, we use obstructed rat models and follow a similar polarized light imaging procedure we developed for normal bladders [13]. We demonstrate that polarized light imaging can locate the obstruction-induced morphological pathology changes in *ex vivo* distended rat bladders. As such, we believe polarized light can potentially be used for *in vivo* regional evaluation of morphology in bladder walls.

2. Materials and methods

2.1 Obstructed and control rat bladders

Female Sprague-Dawley rats with a mass of about 250 g were used in this work according to animal use protocols at Sick Children's Hospital (Toronto, Canada). The rats were divided into two groups: one group for a 2-week obstruction study (6 rats: 3 obstructed and 3 controls) and one for a 6-week obstruction study (6 rats: 3 obstructed and 3 controls). Three rats in each group underwent obstruction surgery as described previously [25]. Briefly, 1) the abdomen was opened and the urethra was ligated with a 0.9 mm steel rod beside it to avoid complete obstruction and attain consistency of the obstruction procedure, 2) the rod was pulled out to enable partial obstruction, and the abdomen was closed. The other three rats in the two cohorts served as controls. For these, the abdomen was opened and closed but no obstruction procedure was performed. The rats' bladders were harvested after 2 weeks and 6 weeks of partial or sham obstruction [13].

Despite the common surgical procedure, the resultant degree of obstruction differed amongst harvested bladders in each group. This may have been due to the slightly different sizes of individual bladders and their outlets, and slight differences in ligating the suture during the surgery. To gauge the resultant obstruction in a rat model, the degree of

#200672 - $15.00 USD Received 6 Nov 2013; revised 9 Jan 2014; accepted 13 Jan 2014; published 27 Jan 2014

obstruction is usually quantified as the ratio of the obstructed bladder mass to the control bladder mass [29,30]. Here, we adopt the same definition to classify the harvested obstructed bladders. Since only the bladder mass itself is of interest and the ureters and urethra in each bladder may differ in mass and size, the ureters and urethra were removed prior to measuring bladder weight.

The bladders were distended using a liquid reservoir coupled to the urethra, as previously described [13]. The liquid is a mixture of Comasi blue dye in ethanol and oil, so as to minimize light penetration to the opposite walls of the bladder. We examined all bladders at a 3.3 kPa pressure, which is close to the maximum physiological pressure experienced by a normal bladder (in both rats and humans). There were two reasons for choosing the highest distension pressure only: 1) the obstructed bladders were under high pressure due to obstruction inside the animal, and thus most would not distend under lower pressures, 2) we were looking for specific anisotropy differences due to obstruction, and performing varying pressure experiments would vary anisotropy due to strain and pressure induced micro-structural changes; as we were only interested in obstruction-induced morphological (anisotropy) changes, one maximum pressure would suffice.

2.2 Measuring anisotropy of bladder wall using polarized light imaging

The distended bladders were imaged in a backscattering geometry (25 degree off axis) using polarized light, as depicted in Fig. 1. As shown, each bladder was suspended such that the imaging plane was parallel to the plane passing through the ureters. The bladders were frequently sprayed with saline to prevent dehydration. The normal bladder volume is small (about 170 μL) and thus the pressure induced by the weight of the filling liquid was negligible compared to the kPa pressure head. Four anatomical regions of each bladder were examined (Fig. 1): dorsal urethral, dorsal dome, ventral urethral and ventral dome.

The imaging apparatus consisted of a light source (laser diode at 635 nm), a rotating polarizer and removable quarter waveplate in both the illumination and collection arms, and a charge coupled device (CCD). Since the collection arm is 25 degree off the excitation axis, no specular reflection reached the CCD. As previously described in detail, the Mueller matrix M of each examined region was obtained from 24 polarimetric measurements (4 different polarization illuminations, with the backscattered light of each illumination analyzed under 6 different polarization collections) [13]. The resultant Mueller matrix, which represents all the polarimetric effects of the tissue, was then decomposed using Lu-Chipman decomposition into three sub-matrices, including the retardance matrix M_R [16]. As explained in our previous papers, the retardance δ is calculated from the M_R as:

$$\delta = \cos^{-1}\{[(M_R(2,2)+M_R(3,3))^2+(M_R(3,2)-M_R(2,3))^2]^{1/2}-1\}, \qquad (1)$$

where $M_R(i,j)$ is the element of M_R in the i^{th} row and j^{th} column. To obtain the retardance orientation (optical axis) θ the matrix M_R is further decomposed to the linear retardance matrix M_{LR} and the optical activity matrix M_ψ. θ the direction of the optical axis projection on the imaging plane can be calculated as:

$$\theta = 0.5\tan^{-1}\left(\frac{M_{LR}(2,3)-M_{LR}(3,2)}{M_{LR}(3,1)-M_{LR}(1,3)}\right), \qquad (2)$$

retardance was then used as a measure of anisotropy in different regions of the bladder wall. However, it should be noted that δ represents the total effect of all anisotropy structures sampled throughout the imaged depth of the wall. Hence, by comparing the regional retardances of obstructed and normal bladders, we are comparing the total morphological changes through the depth; while the morphological changes in some layers might be higher or lower than the rest.

#200672 - $15.00 USD Received 6 Nov 2013; revised 9 Jan 2014; accepted 13 Jan 2014; published 27 Jan 2014

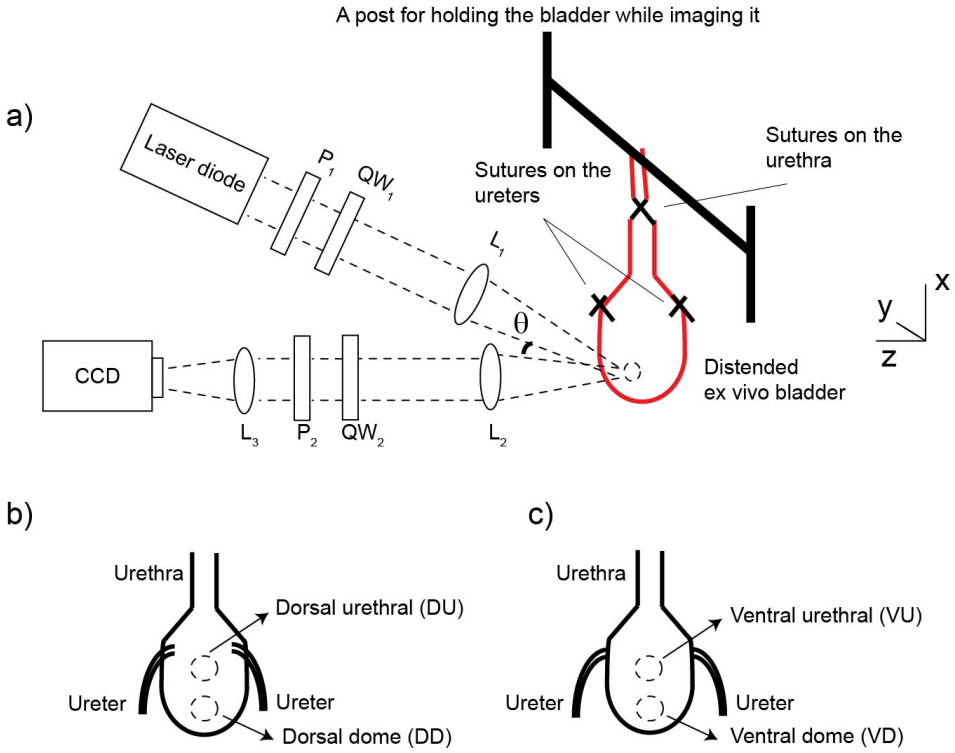

Fig. 1. a) Polarized light imaging set up for examining distended *ex vivo* rat bladders. The ureters and urethra are ligated and the bladder is suspended by the urethra. The CCD and detection arm are along the z-axis, and the illumination arm is $\theta = 25°$ off angle with respect to the detection arm (it is 25° away from the z-axis). P_1 and P_2 are polarizers, QW_1 and QW_2 are quarter waveplates and L_1, L_2 and L_3 are lenses. The image is not to scale. b) Schematic showing the anatomy of the dorsal region of the bladder. Two areas of the dorsal region were imaged: the dorsal urethal (DU) and the dorsal dome (DD). c) Schematic showing the anatomy of the ventral region of the bladder. Two areas of the ventral region were imaged: the ventral urethal (VU) and the ventral dome (VD)

Retardance $\delta = 2\pi \Delta n\, d / \lambda$ is proportional to birefringence Δn and the sampling depth d (related to tissue thickness, its optical properties, and experimental measurement geometry) and inversely proportional to the laser wavelength λ. In previous work, we calculated the bladder wall regional birefringence (by normalizing with optical coherence tomography-measured thickness and Monte Carlo simulated sampling depth) and correlated it with the distension pressure [13]. Here, however, we work with retardance because it is advantageous for potential *in vivo* studies where the thickness of interrogated tissue may be unknown.

3. Results and discussion

The mean masses of obstructed and control bladders in each group are reported in Fig. 2. The bladders in each obstructed group increased more than 150% in mass compared to the controls, which means our surgery resulted in a moderate degree of obstruction compared to other studies [30]. For example, Burmeister et al reported more than 200% increase in mass for the 2-week obstructed bladders relative to the controls, without further increase for the 6-weeks obstruction [30]. Similar trends from 2 to 6 weeks can be noticed in our results as well: as shown in Fig. 2, the mean mass of the 6-week obstructed bladders was more than the mean mass of the 2-week obstructed ones by only ~10%. This minimal increase in mass from 2 weeks to 6 weeks has been previously reported by other groups [29,30]. Another noteworthy finding in Fig. 2 is that the mean mass of the 6-week control bladder was higher than of the 2-week control group, probably due to aging of rats and consequent bladder growth.

#200672 - $15.00 USD Received 6 Nov 2013; revised 9 Jan 2014; accepted 13 Jan 2014; published 27 Jan 2014

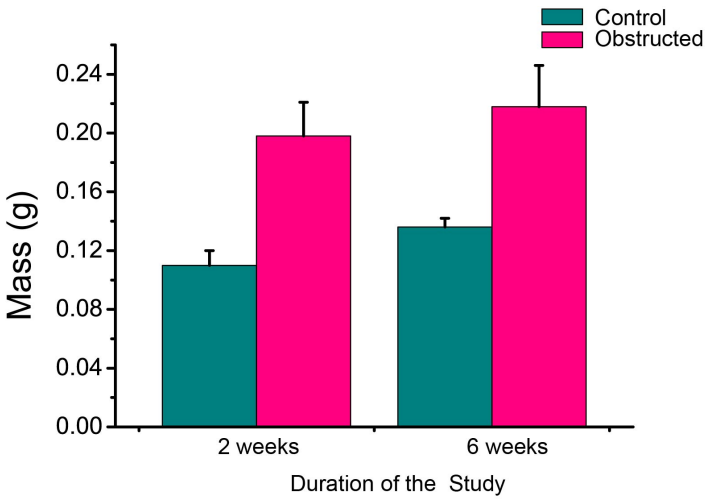

Fig. 2. Mean masses of control and obstructed bladders in the 2 weeks and 6 weeks study. The error bars show the standard deviation from the mean among different bladders.

Next, we investigated the measured regional anisotropy of the bladders from different groups. We emphasize here that the anisotropy detected by polarized light imaging has a distinct and different meaning from the anisotropy measured by biomechanical uniaxial / biaxial stretching tests [11,31]. The biomechanical anisotropy is a measure of how expandable the tissue is in different direction in response to applied forces. Optical anisotropy is an intrinsic asymmetry property of the examined tissue, regardless of whether the tissue is relaxed or stretched. In the case of a distended bladder, it is the total effect of the strain-induced directionality and the intrinsic structure's directionality. A more optically anisotropic bladder wall, at specific distension, may mean fibrosis (more collagen and elastin), more organized extracellular matrix, or muscle hypertrophy (thicker muscle layer) in the wall.

Representative retardance (anisotropy) maps obtained from polarized light imaging and Mueller matrix decomposition from one control and one obstructed *ex vivo* distended bladder in each of the 2-week and 6-week study groups are shown in Fig. 3. The retardance orientation is generally the same across each region, which shows that all bladders are exhibiting some anisotropy (a characteristic of distended bladder at high pressure as previously demonstrated [13]). However, the directionality (magnitude of the anisotropy) in the 6 weeks study seems to be stronger which indicates more organized micro-structure.

#200672 - $15.00 USD Received 6 Nov 2013; revised 9 Jan 2014; accepted 13 Jan 2014; published 27 Jan 2014

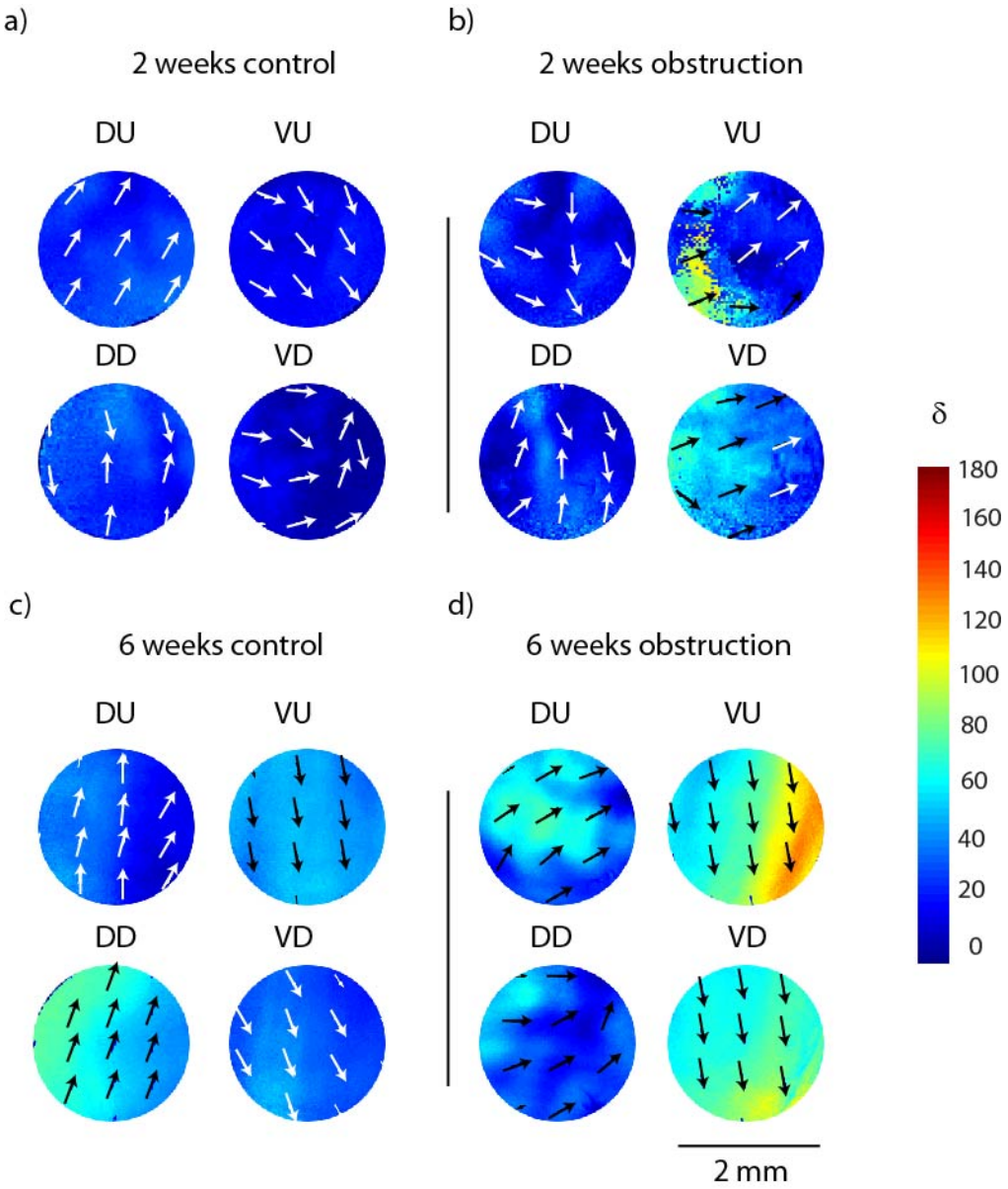

Fig. 3. Representative regional retardances (anisotropy) obtained from polarized light imaging and Mueller matrix decomposition of a) a 2-week control rat bladder, b) a 2-week obstructed bladder, c) a 6-week control bladder, d) a 6-week obstructed bladder. DU = dorsal urethral, DD = dorsal dome, VU = ventral urethral and VD = ventral dome (anatomically depicted in Fig. 1). Color bar shows retardance values in degree and the arrows show the orientation of the retardance (optical axis).

The retardance values were different between individual bladders within the same group, but common trends were present:

1) The control bladders in the 6 weeks study are more anisotropic than controls in the 2 weeks study.

2) Dorsal regions of the control bladder are more anisotropic than the ventral region.

3) Ventral regions are more anisotropic in the obstructed group than controls.

#200672 - $15.00 USD Received 6 Nov 2013; revised 9 Jan 2014; accepted 13 Jan 2014; published 27 Jan 2014

4) The ventral regions of the obstructed bladders are more anisotropic than dorsal regions.

To observe the variation and consistency of these trends among all bladders, and to better identify the significant morphological changes, we quantified the maximum retardance (anisotropy) in all regions of each bladder. The maximum retardance for each region was calculated as follow: 1) each of the images were tiled into small regions of interest (ROI) of 0.2 mm by 0.2 mm; 2) the retardance in each ROI was averaged; 3) the maximum of these averages was used as the maximum retardance for the region. The mean of the regional maximum retardance for all bladders in each group (n = 3) was calculated and plotted, as shown in Fig. 4. The variation among bladders in each group was calculated from the standard deviation of the mean and is indicated by the error bars.

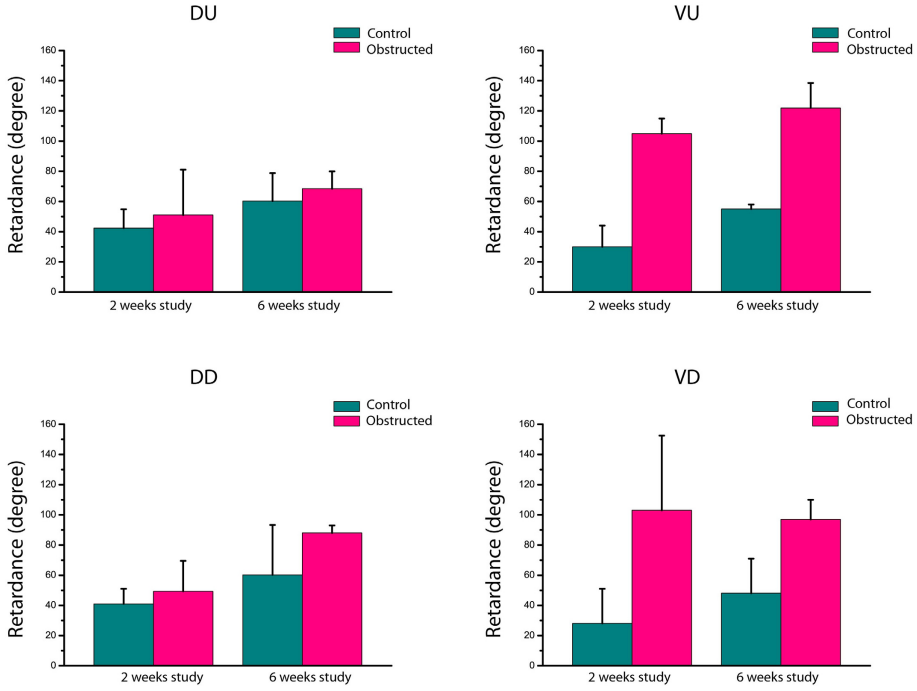

Fig. 4. Mean regional maximum retardance among different rat bladders in each group. The different regions are DU (dorsal urethral), DD (dorsal dome), VU (ventral urethral) and VD (ventral dome). The error bars are the standard deviation from the mean value.

The trend 1) implied from mass changes of Fig. 3 is clear in the anisotropy results of Fig. 4 as well. According to Siroky et al, aging bladders exhibit effects similar to those of obstructed bladders, such as detrusor thickening, fibrosis, and poor contractile response [32]. As discussed earlier, wall thickening and fibrosis can result in higher anisotropy values, which is in agreement with higher anisotropy detected by polarized light in the 6 weeks control bladders compared to the 2 weeks control bladders. This result suggests polarized light may have the potential to detect aging effects in bladders.

The results in Fig. 4 also reinforce the emerging trends 2) and 3). In addition, for both studies (and as expected) the mean value of regional retardance of obstructed bladder is higher than the regional retardance of the control bladders. To evaluate how well the obstruction can be detected using polarized light imaging, we calculated the p-value (from a two-tailed paired t-test) associated with mass and regional retardance differences between normal and obstructed bladders (Table 1).

#200672 - $15.00 USD Received 6 Nov 2013; revised 9 Jan 2014; accepted 13 Jan 2014; published 27 Jan 2014

Table 1. P-values (calculated from paired t-test) for differentiating normal versus obstructed bladders characteristics; δ_{vu}, δ_{VD}, δ_{DU} and δ_{DD} are the retardance of the ventral urethral, ventral dome, dorsal urethral and dorsal dome regions, respectively.

Obstruction study duration	Mass	δ_{VU}	δ_{VD}	δ_{DU}	δ_{DD}
2 weeks	0.04	0.03	0.18	0.92	0.66
6 weeks	0.02	0.03	0.14	0.42	0.39

The following conclusions emerge from the statistical results in Table 1.

1) The retardance of the ventral urethral region can be used to diagnose obstruction (p-value < 0.05).

2) Retardance values in the rest of bladder wall regions are not significantly different between the obstructed and control bladders.

The significant change of retardance in the ventral urethral is reasonable, since the ventral region can anatomically expand more to accommodate a larger volume of urine upon obstruction. In fact, regional differences in response to obstruction have been proposed before by Capelo et al [33] and Schröder et al [34]. For example, Capelo et al showed that the ventral sides of the obstructed bladders become less sensitive to contractile agents (NoRadernaline) [33]. Schröder et al have shown that the serosal layer of the ventral side exhibits greater thickening than that of the dorsal side following obstruction [34]. In another study, Sugimoto et al reported increases of short-length, coiled-shape elastin networks in the bladder neck (the region closer to the urethra) that do not contribute to elasticity; these extracellular matrix changes may be responsible for the anisotropy increase near the urethra that we are observing here [35].

Hence, our results demonstrate relevant significant *regional* anisotropy changes in the obstructed bladder walls, quantified using polarized light imaging and Mueller matrix polar decomposition. Recent studies show that polarized light can be delivered through endoscopic devices for tissue characterization [36,37]. We are currently developing a polarized light probe that can be used through a cystoscope. Having endoscopic polarized light imaging tools, one can potentially identify the regions with maximum retardance changes and then use this information for targeting/ pinpointing / optimizing surgical (augmentation) procedures. As mentioned earlier, currently most augmentation procedures target the dome part of the bladder, whereas our results show that the middle region close to the urethra has the most impaired tissue.

4. Conclusion

Polarized light imaging in combination with Mueller matrix decomposition was used to characterize local structural abnormalities of bladder walls after partial bladder outlet obstruction. A rat model was used for partial bladder outlet obstruction. 2 weeks obstructed (+ control) and 6 weeks obstructed (+ control) *ex vivo* bladders were harvested and distended to the same high (physiologic-level) pressures. Regional maximum retardance values were measured for each bladder wall in the retro-reflection geometry. As suggested by previous studies, the ventral region of the obstructed bladder behaves differently than the control bladders. Our results demonstrate that the retardance (anisotropy) of the ventral urethral regions increases significantly due to obstruction, and the increase follows a similar trend to the bladder mass increase. The increased anisotropy of urethral compared to dome regions may have implications for bladder augmentation surgeries that currently target the dome zones. Interestingly, control bladders of the 6-week study were more anisotropic than control bladders of the 2-week study. These obstructed bladder results are consistent with the presence of fibrosis, muscle hypertrophy and hyperplasia observed previously by other groups. Overall, these findings provide a foundation for investigating *in-vivo* applications of polarimetric imaging for regional pathology detection in urology.

#200672 - $15.00 USD Received 6 Nov 2013; revised 9 Jan 2014; accepted 13 Jan 2014; published 27 Jan 2014